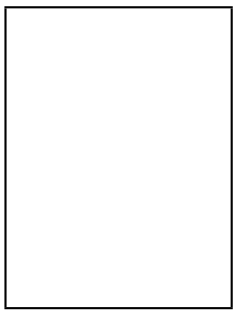

Title: Green Synthesis of SnO_2/Activated Carbon Nanocomposite and Its Application as Photocatalyst in the Degradation of Naproxen

Authors: Shamima Begum, Md. Ahmaruzzaman

PII: S0169-4332(18)30413-6
DOI: https://doi.org/10.1016/j.apsusc.2018.02.069
Reference: APSUSC 38527

To appear in: *APSUSC*

Received date: 29-9-2017
Revised date: 28-1-2018
Accepted date: 6-2-2018

Please cite this article as: Shamima Begum, Md.Ahmaruzzaman, Green Synthesis of SnO2/Activated Carbon Nanocomposite and Its Application as Photocatalyst in the Degradation of Naproxen, Applied Surface Science https://doi.org/10.1016/j.apsusc.2018.02.069

Green Synthesis of SnO_2/Activated Carbon Nanocomposite and Its Application as Photocatalyst in the Degradation of Naproxen

Shamima Begum, Md. Ahmaruzzaman*

Department of Chemistry, National Institute of Technology, Silchar-788010, Assam, India.

*Corresponding author: (Md. Ahmaruzzaman; Email: md_a2002@rediffmail.com)

Graphical abstract

Highlights

- SnO_2/Activated carbon nanocomposite (SnO_2/AC) is obtained using *s*ugarcane juice.
- Activated carbon for the SnO_2/AC is obtained from dried jute stick.
- SnO_2/AC showed excellent photocatalytic activity towards degradation of naproxen.
- Under sunlight, SnO_2/AC shows synergic effect of both adsorption and photodegradation.
- Under sunlight, SnO_2/AC can photocatalytically degrade 94% of NPX.

Abstract

In the current study, SnO_2/Activated carbon (SnO_2/AC) nanocomposites were synthesized by hydrothermal method using $SnCl_4.5H_2O$, *Saccharum officinarum* juice and activated carbon obtained from the dried stem of *Corchorus olitorius*. The biomolecules present in the *Saccharum officinarum* acts as a complexing as well as a capping agent. The size and band gap energy of the as-synthesized SnO_2/AC nanocomposite were found to be 3 nm and 3.6 eV, respectively. Naproxen (NPX) is a widely used nonsteroidal anti-inflammatory drug which is detected both in natural waters and in sewage treatment plant effluents. The synthesized SnO_2/AC nanocomposite shows an invincible photocatalytic property in the degradation of naproxen under direct sunlight. The results showed that 94% of NPX was degraded within 2 h. The degradation of NPX follows pseudo-first-order reaction and the rate of the constant (k) of photodegradation was found to be $2.5x10^{-2}$ min^{-1}. Various parameters, such as effect of catalytic loading, initial concentration, pH and contact time were also studied for optimization of photodegradation process. This study reveals that the synthesized SnO_2/AC nanocatalyst is an excellent photocatalyst for the photodegradation of naproxen from wastewater of pharmaceutical industries due to the synergistic effect of SnO_2 nanoparticles in photocatalysis and activated carbon in adsorption of pollutants. The SnO_2/AC nanocomposite

can be recycled and used upto 5 cycles without any significant alteration in the photocatalytic activity.

Keywords: SnO_2/AC nanocomposite, hydrothermal method, *Saccharum officinarum* juice, *Corchorus olitorius*, Naproxen.

Introduction

During the last two decades, heterogeneous photocatalysis, such as TiO_2, ZnO, and SnO_2 have received great attention due to their potential capability in the field of water purification, photocatalyst, sensor, etc. [1-6]. One of the most lavishly used SnO_2, a metal oxide with rutile crystal structure, owing to its brilliant photocatalytic activity in presence of direct sunlight is widely employed as a photocatalyst in the degradation of harmful organic pollutants [7-9]. It is found that SnO_2 nanostructures are poorly absorbed by the body and shows no significant toxicity nor acts as a carcinogenic agent [10]. From the literature, it is found that SnO_2 nanostructures are widely explored as dye-based solar cells, chemical sensors and as anode for batteries [11-13]. Moreover, in this work, we have chosen SnO_2/AC composite as photocatalyst for the degradation of naproxen. It is found from the literature that SnO_2 nanoparticles have been employed in the degradation of harmful organic compounds from water under direct sunlight. On the other hand, activated carbon is employed as better adsorbents (because of its large surface area, microporous structure and high adsorption capacity) for adsorption of harmful compounds from water. It is also found from the literature, that when this two materials are composited together it shows a synergic effect of both adsorption and photodegradation.So the synthesised SnO_2/AC composite is thought to be the better materials for water treatment (in the degradation of harmful drug naproxen) as it consists of both SnO_2 nanoparticles and activated carbon**.**

In order to increase the utilization efficiency of SnO_2 as a photocatalyst, various research works on the band gap tailoring are investigated to minimize forbidden bandwidth and electrons-holes recombination of metal oxide nanoparticles [14]. Keeping in view of the above, various nanostructured composites materials, such as metal/metal oxide, metal oxide/metal oxide, and non-metal/metal oxide have been developed [15-17]. The carbon materials, such as activated carbon (AC) as non-metal fabrication on metal oxide is recently explored in various research works because of its excellent properties, such as decreasing the band gap energy of SnO_2 and increasing active site which can improve its photocatalytic activity [18]. It is observed that metal oxide fabricated on AC shows a synergistic effect of AC in adsorption and metal oxide on photodegradation of harmful pollutants [17].

Some successful methods were employed for the synthesis of nanostructured composites materials using sol-gel, microwave, spray pyrolysis, hydrothermal and chemical precipitation route [19-21]. However, since last few decades efforts were made to synthesize nanomaterials using eco-friendly and environmentally benign raw material which is also cost-effective. Therefore, in the present work, we have synthesized SnO_2/AC nanocomposite following hydrothermal route using *Saccharum officinarum* juice as a capping and complexing agents, as it contains various amino acids and organic acids and inorganic salts [22]. The activated carbon (AC) is obtained from the chemical activation of the agricultural waste dried stem of *Corchorus olitorius*. Therefore, it is for the first time, the synthesis of SnO_2/AC nanocomposite using *Saccharum officinarum* juice and *Corchorus olitorius* stem has been reported in this investigation.

Now-a-days, pharmaceutical wastes are considered as organic micropollutants (OMPs) in surface waters [23]. The commonly reported OMPs present in municipal wastewater streams are the pharmaceutically active compounds (PhACs) [24]. There is a possible risk of human and nature due to the presence of this PhACs in aquatic environment [25]. These PhACs and

their metabolites are found in the environment because of their improper disposal of expired and unused medicine [26-28]. Therefore, its removal from the environment is a challenge for the researchers. Among these harmful pharmaceutical wastes, naproxen (NPX) is a nonsteroidal anti-inflammatory drug (NSAID) which is used as an analgesic and antipyretic drug for the treatment of rheumatoid arthritis [29-31]. Though, naproxen, not toxic if it is present by itself but prolong accumulation in water and soil can cause long-term toxic effects [32]. The removal of these pharmaceuticals from water is very important in order to have a sustainability of nature and ecosystem. Pharmaceutical drugs can be removed from aqueous environment by photodegradation process using sunlight, UV lamps and xenon lamp [33-36]. Semiconductor nanoparticles, such as ZnO and TiO_2 have been widely employed for the degradation of naproxen (NPX) [37, 38]. In the current study, synthesized SnO_2/AC nanocomposite is employed for photodegradation of this harmful toxic drug, naproxen (NPX) from aqueous solution under direct sunlight. The photodegradation of naproxen by using SnO_2/AC nanocomposite as a catalyst is reported for the first time in this study.

2. Experiment

2.1. Materials

Stannic chloride pentahydrate ($SnCl_4.5H_2O$), concentrated phosphoric acid (H_3PO_4) and naproxen drug were of analytical grade and purchased from Sigma-Aldrich, India. Double distilled water was used as a solvent in all the experimental studies.

2.2. Synthesis of SnO2/Activated Carbon Nanocomposite

2.2.1. Preparation of activated carbon

Activated carbon (AC) is prepared by chemical activation of *Corchorus olitorius* stems which are collected from a nearby village. *Corchorus olitorius* stems were washed thoroughly with distilled water and dried at 100ºC for 24 h in a hot air oven. Then, the precursors were

impregnated with phosphoric acid (H_3PO_4) solution at an impregnation ratio of 1:1 (by weight) and heated for 1 h with continuous stirring for uniform distribution. The mixture was treated in a muffle furnace at a temperature of 400 ºC for 2 h. The product so obtained was washed several times with distilled water till the pH is neutral. Then the final product was dried and grounded into fine uniform particles.

2.2.2. Preparation of *Saccharum officinarum* juice

Saccharum officinarum (sugar cane) stems were collected from a local field and its juice was extracted by crushing its stems in two roller crusher machine owned by a local vendor. The collected juice was filtered through a Whatmann filter paper no. 41 and a 10% aqueous solution of juice is prepared.

2.2.3. Preparation of SnO_2/AC nanocomposite

Hydrothermal route is followed for the synthesis of SnO_2/AC nanocomposite. In this method, 10% sugarcane juice (10 mL of sugarcane juice in 90 mL distilled water) was added dropwise with continuously stirring into a 0.1 M aqueous solution of $SnCl_4.5H_2O$. Then a required amount of the prepared AC is added (1:1 ratio by weight of Sn:AC) and the mixture is continuously stirred for 15 min. Then the reaction mixture was transferred into a 150 ml Teflon lined autoclave and sealed tightly. The sealed autoclave containing reaction mixture is kept in a hot air oven at 100˚C for 6 h. These results into the formation of a grey precipitate and kept this precipitate at room temperature for 24 h to get matured. Then the resulting precipitate is washed thoroughly several times with distilled water for the removal of any impurities or untreated product left and then dried in a hot air oven at 60 ˚C for 12 h. The greyish powder so obtained is marked as SnO_2/AC and kept in an airtight container until further use.

2.3. Characterization of Synthesized SnO_2/Activated Carbon nanocomposite

The size and morphological study of the synthesized SnO_2/Activated carbon (SnO_2/AC) nanocomposite before and after photodegradation were determined by using JEM-2100 Transmission Electron instrument. Powder X-ray diffraction of the synthesized SnO_2/AC nanocomposite before and after photodegradation was performed using Phillips X'Pert PRO diffractometer with Cu Kα radiation of wavelength 1.5418Å. Further, for the functional group study of the synthesized SnO_2/AC nanocatalyst infrared (FT-IR) spectra were recorded in the wave number range from 400 to 4000 cm^{-1} by Bruker Hyperion 3000 FTIR spectrometer. EDX analysis was performed using energy dispersive spectrometer (OxfordXmax 20) for chemical composition study. All the studies of UV absorption are performed in Genesys 10S UV-vis spectrophotometer operational with 1 cm quartz cell from wavelength between 200 nm to 400 nm at a speed of 600 nm/min.

2.4. Photocatalytic degradation of Naproxen

For the study of the photocatalytic activity of SnO_2/AC nanocomposite for the degradation of naproxen drug (NPX), various investigations were performed in different batches for the establishment of optimum experimental conditions under direct solar irradiation. For the photodegradation study of NPX solution, a known amount (5-50mg/L) of the synthesized nanocatalyst was dispersed in 50 mL of various concentrations (5, 10, 15, 20 and 25 mg/L) of NPX solution in different borosil conical flasks of capacity 100 mL. The solution mixtures were kept on a magnetic stirrer with continuous stirring in dark for 2 h before solar irradiation for the adsorption/ desorption equilibrium. Then, the conical flasks containing the solution mixtures were kept under direct sunlight with continuous stirring until the maximum degradation is reached. The solar irradiation was carried out on a Sunny day from 10:00 am to 12:00 am on March 2017 at NIT Silchar campus. Then, at after every constant interval of time, one of the flasks containing solution mixture was taken off from the sunlight irradiation and 2 ml of the solution mixture was withdrawn from it in a conical flask. The withdrawn

samples were further centrifuged to remove the catalyst if any present in it and the supernatant was monitored in a UV-vis spectrophotometer to determine the concentration of remaining NPX drug present in the solution mixtures. Here, in this study, the changes in the UV-vis absorption peak of naproxen at 230 nm are taken into account. This procedure is continued until maximum degradation of NPX drug is achieved under sunlight. For comparative study, a similar experiment was conducted in parallel with blank solutions of NPX drug i.e without the presence of a catalyst under direct sunlight for the same interval of time as that of with catalyst. The percentage degradation efficiency of NPX was calculated using the following equation:

Percentage efficiency (%) = $[(C_0 - C)/C_0] \times 100$…….. (1)

where C_o and C are the concentration of NPX drug in mg/L solution at initial and after photocatalysis at time t, respectively.

2.5. Recyclability of the photocatalyst

To exhibit the longevity of the synthesized nanocatalyst, recyclability of the catalyst is very important factor. Therefore, a reusability test of the exhausted SnO_2/AC nanocatalyst was executed after the completion of photodegradation process. To recover the photocatalyst after photodegradation process, used catalyst was collected by centrifugation and was passed through Whatman No. 41. It was further washed with hot water several times and finally, with acetone and then dried in a hot air oven at 60º C for 3 h. Finally, the used catalyst was recovered and employed again for the photocatalytic degradation of NPX. The percentage degradation efficiency of NPX was noted using equation 1.

3.1. Characterization of the photocatalyst

3.1.1. UV-visible studies:

The UV-vis absorption spectrum the synthesized SnO_2/AC nanocomposite carried out at room temperature is represented in figure 1a. Figure 1a shows no prominent absorption peak. From the UV absorption spectrum of SnO_2/AC nanocomposite, the optical band-gap energy (E_g) was calculated by using the equation, $\alpha(v)h\nu$ = K ($h\upsilon - E_g$) ^{n}, where, hυ is the photoenergy, K is constant, α(ν) is the absorption coefficient. The value of 'n' varies with different type of transition, here in this study, the value of n is ½ for allowed direct transition. The calculated band gap energy is found to be 3.6 eV which is obtained by the extrapolation of $(\alpha h\nu)^2$ versus (hν) curve as shown in figure 1b. The band gap is almost similar to that of bulk SnO_2 which makes it a better photocatalyst as compared to usual SnO_2 nanoparticles whose band gap is higher. The lower band gap value is favorable for photocatalytic activity.

3.1.2. XRD studies

The XRD pattern of prepared SnO_2/AC nanocomposites is represented in Figure 2. The XRD pattern of SnO_2/AC nanocomposites shows peaks at 2θ values of around 26.49º, 33.8º, 51.67º and 65.81º. This indicates the presence of SnO_2 as these peaks are assigned to the (110), (101), (211) and (301) planes of standard tetragonal structured SnO_2 (JCPDS 41-1445), respectively. Since the AC also shows peaks at around 2θ=26.4º and 65.83º which corresponds to (111) and (122) plane of carbon (JCPDS 75-0444), respectively. Therefore, all the peaks of carbon coincide with that of SnO_2 and no separate peak for AC is observed. From XRD data, average crystallite can be calculated from the full width at half maximum (FWHM) of the diffraction peak using the Debye-Scherrer equation:

$$D = \frac{k\lambda}{\beta Cos\theta} \quad \text{..... (2)}$$

where D is taken as the crystallite size in nm, λ is the diffraction wavelength in Å, β is the FWHM in radian, θ is the diffraction angle in (˚) degree and K is a constant which also called

shape factor and its value is close to unity. Therefore, using the given equation, the calculated average crystallite size of the synthesized SnO_2/AC is found to be 3 nm.

3.1.3. TEM, HRTEM and SAED studies

The morphology, size distribution and microstructure of the synthesized SnO_2/AC nanocomposite were scrutinized by TEM and HRTEM images. Figure 3a illustrates TEM image of SnO_2/AC nanocomposite, from which the average size of the particles was calculated and found to be 3 nm. Figure 3d represents the particle size distribution of SnO_2/AC nanocomposite in the form of the histogram which is evaluated from the TEM image. The histogram shows that the average size is 3 nm. From HRTEM image of SnO_2/AC nanocomposite represented in figure 3b, it is observed that shape of the particles is non-uniformly distributed i.e. some particles are non-spherical irregular in shape and some are spherical in shape. From the HRTEM images, the lattice fringes were also calculated and found to have lattice spacing of 0.27 nm which corresponds to (101) lattice plane of typical SnO_2(JCPDS 41-1445). The SAED pattern of SnO_2/AC nanocomposite represented in figure 3c shows numbers of concentric diffraction ring. From the diffraction rings the d-spacings were calculated and establish that the entire planes go well with the (110), (101), (211) and (301) plane of SnO_2 (JCPDS 41-1445). Therefore, the average crystallite size calculated from the XRD patterns comes to a good agreement with the average particle size measured from TEM image of SnO_2/AC nanocomposite.

3.1.4. FTIR analysis

The FTIR spectra of *Saccharum officinarum* juice, activated carbon (AC) and the prepared SnO_2/AC nanocomposite are shown in Figure 4. The functional groups present in the nanocomposite can be inspected from the FTIR spectra. The FTIR spectra of *Saccharum officinarum* juice shows several bands, however, some seems to be an important band as it takes part in the synthesis of SnO_2/AC nanocomposite. One of such band appeared at 1033

cm^{-1} which is due to the C–H in-plane deformation in syringyl unit of lignin present in Saccharum officinarum which might get extracted into the juice [39]. The band at 1413 cm^{-1} is assigned to C–H bending vibrations of the aliphatic alkyl chain present in the juice organic salt. The strong band at 1613 cm^{-1} is attributed to C=O stretch of biomolecules, such as amides amino acids or some organic acids, monosaccharides, etc. containing –COO group present in the *Saccharum officinarum* juice [40, 41].

The FTIR spectra of AC shows only two bands at 1171 and 1580 cm^{-1} which attributes to C-O stretches and C=C stretches and may be due to the functional group present in the *Corchorus olitorius* stem.

The FTIR of SnO_2/AC nanocomposite shows the existence of a prominent band at 625 cm^{-1} which may be due to the Sn-O-Sn anti-symmetric vibrations. The band at 1033 cm^{-1} which is due to the C–H in-plane deformation in syringyl unit of lignin present in Saccharum officinarum arises due to the residue of *Saccharum officinarum* juice which is present on the surface of the nanocomposite The band at 1460 cm^{-1} is assigned to C–H deformation which may arise due to the interaction with the Saccharum officinarum juice. Here, it is found that the said band is shifted and may indicate that this functional group is involved in the formation of SnO_2/AC nanocomposite. The band at around 1622 cm^{-1} is attributed to C=O stretch of biomolecules seems to shift in the case of the nanocomposite. This may be due to the fact that this functional group takes part in the process of synthesis of the nanocomposite. The band at 3430 cm^{-1} is due to the stretching vibrations of -OH groups present on the surface of the nanocomposite. The band at 2923 cm^{-1} is assigned to C–H stretching which may be due to the interaction of the alkyl chain present in the *Saccharum officinarum* juice. Neither strong impurity band nor any unwanted noise is observed in the as-synthesized SnO_2/AC nanocomposite.

3.1.5. EDX analysis

From the EDX spectrum, the chemical composition of SnO_2/AC nanocomposite can be examined. The EDX spectrum represented in Figure 5 shows strong signals in the Sn, O and C region. The signal approximately at around 3.1, 3.4, 3.7 and 3.9 KeV is due to the presence of Sn, the two signals around 0.1 keV and 0.5 keV correspond to C of activated carbon and O of SnO_2. Cu grid was used for the analysis of the synthesized SnO_2/AC nanocomposite and therefore, a weak signal for Cu at around 1 keV is observed. Another, two weak signals are also observed at around 1.3 and 1.7 keV which may be due to the presence of Mg and Si in the Cu grid as an impurity. Therefore, the presence of these three elements can be neglected. The elemental compositions of the synthesized SnO_2/AC nanocomposite (obtained from EDX analysis) are depicted in Table 1. The predominant signals for C, O and Sn and also the quantitative study (shown in Table 1) confirm the formation of SnO_2/AC nanocomposite.

3.2. Role of *Saccharum officinarum* juice

The *Saccharum officinarum* juice contains various biomolecules, such as amino acids, monosaccharides, disaccharides, polysaccharides and organic acids. These biomolecules act as a complexing and capping agent in the synthesis of SnO_2/AC nanocomposite [40]. During the hydrothermal synthesis route, Sn^{+4} ion may form a complex with the amino acids and other organic acids which further results in the formation of SnO_2/AC. In fact, it is the biomolecules present in *Saccharum officinarum* juice which behaves as a ligand and can associates along with the precursor metal ion forming complex [41,42]. These biomolecules also get adsorbed on the surface of SnO_2/AC and suppressed the growth of the nucleated particles and ultimately led to the formation of the nanocomposite. Thus, these biomolecules not only acts as a complexing agent but also acts as a good capping agent which inhibit grains from overgrowth and aggregation. The steric repulsive forces between the nucleated ligands help in preventing the aggregation of particles. Therefore, these biomolecules present in the

Saccharum officinarum juice engaged in dual role i.e. as a complexing agent as well as capping agent in the biosynthesis of SnO_2/AC nanocomposite. The presence of biomolecules, such as amino acids, organic acids, proteins, monosaccharides, and polysaccharides on the surface of SnO_2/AC nanocomposite is observed in the FTIR spectrum and confirms the role of amino acids, carbohydrates and other biomolecules present in *Saccharum officinarum* juice in the formation of SnO_2/AC nanocomposite.

3.3. Assessment of photocatalytic activity of the synthesized SnO_2/AC nanocomposite

To determine the photocatalytic activity of the synthesized SnO_2/AC nanocomposite, the change in optical absorption at 230 nm of NPX solutions are recorded during the photodegradation process. Adsorption/desorption studies of naproxen were carried out for 120 min in the dark. From the dark study, it is found that around 10% of the NPX was removed due to adsorption in 60 min and further no removal of NPX was observed. Therefore, in all the optimization study, the solution mixture was kept in dark for 60 min and removal of NPX due to adsorption is neglected. The following investigations were performed for the optimization of catalyst for a better result with minimum dose and time:

3.3.1. Effect of catalyst loading

To avoid the redundant use of photocatalysts, it is very important to determine the optimum catalyst loading so that catalyst is used at its best with maximum photodegradation efficiency. Figure 6a shows the effect of catalyst loading on the degradation of NPX drug solution. To determine the optimum dose of catalyst, experiments were run with varying dose of catalyst from 5-50 mg/L in 50 ml of NPX solution under direct sunlight keeping the concentration of NPX and pH of the solution constant i.e. 10 mg/L at a pH of 4. The maximum percentage removal of NPX was observed at a catalyst dose of 30 mg/L and after that almost no degradation is observed at a higher dose. The number of availability of active site increases with higher catalyst loading and at the same time solution opacity was also increased and

hence, results in the shielding effect. Therefore, the penetration of radiation through the suspension decreases, and thereby, the photocatalytic activity of the catalyst get decreased, as the surface of the catalyst cannot be activated due to which production of active radicals is reduced.

3.3.2. Effect of initial NPX concentration

To determine the effect of initial concentration of NPX, photodegradation experiments were performed with varying concentrations of NPX solution of 5, 10, 15, 20 and 25 mg/L and keeping a fixed catalytic dose of 30 mg/L and constant pH. The study shows that the highest degradation efficiency was observed at 5 mg/L of NPX solution which is depicted in figure 6b. It is observed that the percentage of NPX degradation is decreased as the concentration of NPX is increased. This decrease in photodegradation is due to the obstruction of light penetration into the solution, as the path length of photons entering the solution decreases with increase in concentration [43]. Further, the higher the initial concentration of NPX, greater catalyst surface area is required for degradation of NPX. This also leads to additional catalyst loading which ultimately results in increasing opacity of the solution [35]. Therefore, the minimal optimum concentration of NPX solution is required for bettter photodegradation efficiency**.**

3.3.3. Effect of pH

To determine the effect of pH (2–9), photodegradation experiments were run by keeping a fixed dose 30 mg/L of SnO_2/AC photocatalyst in 50 mL of NPX solution (concentration is fixed at 5 mg/L) under direct sunlight. Photodegradation of NPX was examined in both acidic and basic mediums by adjusting the pH with the help of 0.1 M/0.01M HCl and NaOH. Figure 6c shows the effect of pH on the solar degradation of NPX. It is observed that in the acidic pH range (2-5) maximum degradation is obtained at a pH of 3 and after that degradation efficiency is significantly decreased at high pH ranges (7-9). This may be due to the fact that

naproxen solutions exists in protonated and deprotonated forms at a pH of 3 and 5 and at a pH of 7 and 9, it is nearly fully deprotonated [44]. So, it is unfavourable for direct and indirect photodegradation of naproxen when it is in the deprotonated state. Therefore, pH is an important parameter for the degradation of naproxen, as low pH value facilitates the degradation of naproxen [45].

3.3.4. Effect of contact time

Figure 6d represents the effect of optimum contact time for the photodegradation of NPX under direct sunlight. To determine the optimum contact time for the photodegradation of NPX under direct sunlight, the experiments were carried out with the optimum loading of 30 mg/L of SnO_2/AC nanocomposite dose in 50 mL of 5 mg/L of NPX solution at a pH of 3 under direct solar irradiation. After every 10 min of interval of time, the change in UV-vis absorption of NPX at 230 nm is recorded until maximum degradation is observed. From the assessment, it is observed that on increasing the contact time, photodegradation increases up to 94% at 120 min and the UV absorption peak at 230 nm becomes almost flat. After 120 min of degradation, no notable difference in the percentage removal was observed. This hindrance in further degradation of NPX and may be due to the fact the surface of the nanocomposite gets saturated so no active site is available for further photodegradation of NPX. Therefore, SnO_2/AC nanocomposites were found to degrade 94% of naproxen under optimization process parameters (concentration, 5 mg/L of naproxen; optimum dose of 30 mg/L; time, 120 min; and pH, 3).

3.3.5. Photodegradation study of NPX by SnO_2/AC nanocomposite

In order to determine the effect of degradation of NPX in various conditions two parallel experimental sets were run by taking 50 mL of 5 mg/L of naproxen at pH of 3. In one set of the experiment, no catalyst was added and 30 mg/L of SnO_2/AC nanocatalyst was dispersed in another set. Both the sets of solution mixture were kept in dark for 120 min for adsorption

and desorption equilibrium and after that, both the reaction mixtures were irradiated with direct sunlight for the photodegradation study. Figure 7a shows a comparative study in dark and under sunlight with and without a catalyst. After every regular interval of time, one conical flask is taken out and the UV-vis absorption of the solution was recorded. It is found the solutions without catalyst shows no degradation of naproxen in the dark condition. Whereas, the solution mixture containing SnO_2/AC nanocatalyst showed around 10% removal of naproxen within 60 min. This may be due to adsorption by AC present in SnO_2/AC nanocatalyst and no significant removal of naproxen was observed after 60 min. Then, both the reaction mixtures were brought under direct sunlight for photodegradation study. After every regular interval of time, the UV-vis absorption peak of NPX was recorded for both the solutions and depicted in figure 7b. It was found that the solution containing only NPX solution with no catalyst shows only 2% removal after 120 min, whereas solution containing SnO_2/AC nanocatalyst showed 94% degradation as shown in figure 7c.

The catalytic activity of SnO_2/AC nanocomposite was determined from the kinetics of of degradation of naproxen. It is found that it follows pseudo-first-order kinetics model. The rate of the reaction can be obtained using Langmuir-Hinshelwood equation:

$$\ln(C_0/C) = kt \qquad 3$$

where k is the rate constant, C_o and C are absorbance or concentration before and after photodegradation of NPX, respectively. From equation (3), rate constant can be obtained by applying linear correlation. The plot of ln (C_0/C) versus irradiation time, t, is shown in figure 7d. The rate constant k (min^{-1}) for the degradation of NPX is calculated and found to be $2.5x10^{-2}$ min^{-1}. The increased rate constant (k) value suggests that the SnO_2/AC nanocomposites act as an excellent photocatalyst due to the synergistic effect of SnO_2 in photodegradation and AC in adsorption.

3.4 Mechanism of Photodegradation of NPX by SnO_2/AC nanocomposite under direct sunlight

The photocatalytic activity of a semiconductor nanostructured materials is mainly based on the generation of the electron-hole pair, when a light energy greater than its band gap energy falls onto it. The probable mechanism of photocatalytic activity of SnO_2/AC nanocomposite on the degradation of naproxen is shown in figure 8. When the sunlight falls on the SnO_2/AC nanocomposite, the electrons present on the valance band get excited and jump onto the conduction band and then migrate to the particle surface (eqn. 4). The photogenerated electrons move towards the AC surface which acts as a trap and thus prevents from quick recombination of photogenerated electron-hole pairs [46]. Therefore, no recombination of hole-electron takes place [14]. The electrons are reduced O_2 and generates $O_2^{-\cdot}$ (eqn. 5). No recombination of hole-electron is occured, as the hole also moves to the particle surface and helps in the generation of $OH^{\bullet}$ radical by reacting with H_2O (eqn 6). The $OH^{\bullet}$ radical so formed is a powerful oxidizing agent and attack organic molecules of the pollutant resulting an effective removal of NPX from the water in the form degradation products (eqn.7) [47]. The photocatalytic degradation mechanism of NPX by SnO_2/AC nanocomposite can be proposed as shown below [14]:

$$SnO_2/AC + h\nu \rightarrow SnO_2/AC\ (e^-_{CB} + h^+_{VB}) \quad (4)$$

$$SnO_2/AC\ (e^-_{CB}) + O_2 \rightarrow SnO_2/AC + O_2^{\bullet -} \quad (5)$$

$$SnO_2/AC\ (h^+_{VB}) + H_2O \rightarrow SnO_2/AC + HO^{\bullet} + H^+ \quad (6)$$

$$SnO_2/AC\ (h^+_{VB}),\ HO^{\bullet} + CBZ \rightarrow \text{degradation products} \quad (7)$$

The SnO_2/AC nanocomposite exhibited better photocatalytic degradation efficiency because of two factors: Firstly, AC results in the formation of smaller particle size and thus provides a large surface area on the photocatalyst. Thus, more active sites will be available which leads to an increase in the adsorption of O_2 and H_2O, and hence increase in the generation of

radicals [48] and secondly, AC may lead to the adsorption of the drug molecule due to which the availability of the drug molecule on the surface of the photocatalyst is more and thereby results in faster and better photodegradation efficiency [46, 49]. A large number of SnO_2 NPs may be spread on the surface of AC which gives rise to more activation time which in turn results in the availability of a more active site on the surface of AC. This may also contribute to the higher photocatalytic activity of SnO_2/AC nanocomposite. Herein, the SnO_2/AC nanocomposite seems to show a synergistic effect due to the combination of the adsorption capacity of the AC and the photocatalytic activity of SnO_2 [14].

3.5. Reusability of the photocatalyst

An excellent catalyst is expected to have a good durability with the high-efficiency on back to back multiple cycles of the experiment. Therefore, assessment of the efficiency of the catalyst is a significant factor. A reusability test was performed in order to determine the durability of the synthesized SnO_2/AC nanocatalyst and how many cycles of the experiment can be run with maximum photocatalytic activity. The recovered catalysts were used again for the next run of the photocatalytic process. This process is repeatedly performed up to 5 cycles and after every cycle of an experimental run, photocatalytic efficiency is calculated using equation 1. There was no significant loss in catalytic activity, however, in the last cycle, a negligible loss in catalytic activity was observed as shown in figure 9. Therefore, we can say that the SnO_2/AC nanocomposite is an excellent photocatalyst for the degradation of NPX. The recovered catalyst was further characterized by XRD and TEM analysis in order to determine the stability and morphological changes occurred. Figure 10a and b shows that XRD and TEM image of the recovered SnO_2/AC nanocomposite. It is observed from XRD pattern of the figure 10a that all the crystallographic planes after degradation remained same as that of before photocatalysis. Again from the TEM image of figure 10b, it is found that neither significant change in size or morphology nor any further agglomeration is observed.

Therefore, we can say that SnO_2 NPs composited with AC results in an efficient and reclaimable photocatalyst.

4. Conclusion

In conclusion, it is found that an efficient and reclaimable SnO_2/AC nanocomposite was synthesized following hydrothermal route by employing green, environmentally benign and cost-effective raw material, Saccharum officinarum juice and *Corchorus olitorius* stem. It is confirmed by TEM images and XRD patterns that size of the synthesized SnO_2/AC nanocomposite is 3 nm. It is also found that band gap energy can be successfully tuned and reduced to 3.6 eV which is very close to band gap energy of bulk SnO_2. This reduced band gap energy makes the synthesized nanocomposite a brilliant photocatalyst under direct sunlight.

From the optimization study of the photocatalyst, it showed that a dose of 30 mg/L of prepared SnO_2/AC nanocomposite can degrade 94% of 5 mg/L NPX solution within 120 min at a pH of 3 under direct sunlight. The kinetic study shows a high rate constant of 2.5 $x10^{-2}$ min^{-1} which may be due to the synergistic effect of SnO_2 and AC which makes the SnO_2/AC nanocomposite an excellent photocatalyst. The reusability study of the SnO_2/AC nanocomposite shows that it can be used upto 5 cycles without any significant decrease in photocatalytic activity. Further, it is confirmed by the TEM images and XRD patterns of the recycled SnO_2/AC nanocomposite, as it showed no significant changes in its structural and morphological properties.

Acknowledgements

We would like to thank the Director, NIT Silchar for providing lab facilities and scholarship. We would also like to acknowledge SAIF-NEHU, IIT Bombay and CSMCRI Bhavnagar for providing TEM, IR, EDX and XRD data.

References

[1] Mora-Sero, I., Bisquert, J., Dittrich, T., Belaidi, A., Susha, A.S., Rogach, A.L., 2007. Photosensitization of TiO_2 Layers with CdSe Quantum Dots: Correlation between LightAbsorption and Photoinjection, J. Phys. Chem. C 111, 14889-14892.

[2] Umetsu , M., Mizuta, M., Tsumoto, K., Ohara , S., Takami, S., Watanabe, H., Kumagai, I., Adschiri, T., 2005. Bio-assisted room-temperature immobilization and mineralization of zinc oxide-The structural ordering of ZnO nanoparticles into a flower-type morphology. Adv. Mater.17, 2571–2575.

[3] Prakash, K., Senthil Kumar, P., Pandiaraj, S., Saravanakumar, K., and Karuthapandian, S., 2016. Controllable synthesis of SnO_2 photocatalyst with superior photocatalytic activity for the degradation of methylene blue dye solution. J. Exp. Nanosci. 8080, 1–18.

[4] Kim, S.P., Choi, M.Y., and Choi, H.C., 2016. Photocatalytic activity of SnO_2 nanoparticles in methylene blue degradation.Mater. Res. Bull. 74, 85–89.

[5] Sberveglieri, G., 1992. Classical and novel techniques for the preparation of SnO_2 thin-film gas sensors. Sens. Actuators B 6, 239-247.

[6] Li, F., Xu, J., Yu, X., Chen, L., Zhu, J., Yang, Z., Xin, X., 2002. One-step solid-state reaction synthesis and gas sensing property of tin oxide nanoparticles. Sens. Actuators B 81, 165–169.

[7] Bhattacharjee, A., and Ahmaruzzaman, M., 2015. A green and novel approach for the synthesis of SnO_2 nanoparticles and its exploitation as a catalyst in the degradation of methylene blue under solar radiation. Mater. Lett., 145, 74–78.

[8] Bhattacharjee, A., Ahmaruzzaman, M., and Sinha, T., 2015. A novel approach for the synthesis of SnO_2 nanoparticles and its application as a catalyst in the reduction and photodegradation of organic compounds. Spectrochim Acta A Mol Biomol Spectrosc., 136, 751–760.

[9] Bhattacharjee, A., and Ahmaruzzaman, M., 2015. A novel and green process for the production of tin oxide quantum dots and its application as a photocatalyst for the degradation of dyes from aqueous phase. J. Colloid Interface Sci., 448, 130–139.

[10] Begum, S., Devi, T.B., Ahmaruzzaman, M., 2016. L-lysine monohydrate mediated facile and environment friendly synthesis of SnO_2 nanoparticles and their prospective applications as a catalyst for the reduction and photodegradation of aromatic compounds. J. Environ. Chem. Eng. 4, 2976–2989.

[11] Shang, G., Wu, Huang, J.M., Lin, J., Lan, Z., Huang, Y., Fan, L., 2012. Facile synthesis of mesoporous tin oxide spheres and their applications in dye-sensitized solar cells. J. Phys. Chem. C 116, 20140–20145.

[12] Phadungdhitidhada, S., Thanasanvorakun, S., Mangkorntong, P., Choopun, S., Mangkorntong, N., Wongratanaphisan, D., 2011. SnO_2 nanowires mixed nanodendrites for high ethanol sensor response. Curr. Appl. Phys., 11, 1368–1373

[13] Feng, L., Xuan, Z., Ji, S., Min, W., Zhao, H., Gao, H., 2015. Preparation of SnO_2 Nanoparticle and Performance as Lithium- ion Battery Anode. Int. J. Electrochem Sci., 10, 2370–2376.

[14] Ragupathy, S., Sathya, T., 2011. Synthesis and characterization of SnO_2 loaded on groundnut shell activated carbon and photocatalytic activity on MB dye under sunlight radiation. J. Mater. Sci. Mater. Electron., 27, 5770–5778.

[15] Guo, J., Guo, M., Jia, D., Song, X., Tong, F., 2016. CdS loaded on coal based activated carbon nanofibers with enhanced photocatalytic property. Chem. Phys. Lett., 659, 66–69.

[16] Muthirulan, P., Meenakshisundararam, M., Kannan, N., 2013. Beneficial role of ZnO photocatalyst supported with porous activated carbon for the mineralization of alizarin cyanin green dye in aqueous solution. J. Adv. Res., 4(6), 479–484.

[17] Meng, H., Hou, W., Xu, X., Xu, J., Zhang, X., 2014. TiO2-loaded activated carbon fiber: Hydrothermal synthesis, adsorption properties and photo catalytic activity under visible light irradiation. Particuology, 14, 38–43.

[18] Ghaedi, M., Karimi, H., Yousefi, F., 2014. Silver and zinc oxide nanostructures loaded on activated carbon as new adsorbents for removal of methylene green: A comparative study, Hum Exp Toxicol, 33, 1–12.

[19] Begum, S., Devi, T.B., Ahmaruzzaman, M., 2016. Surfactant mediated facile fabrication of SnO_2 quantum dots and their degradation behavior of humic acid. Mater.Lett. 185, 123–126.

[20] Muneer, I., Farrukh, M.A., Javaid, S., Shahid, M., Khaleeq-ur-Rahman, M., 2015. Synthesis of Gd_2O_3/Sm_2O_3 nanocomposite via sonication and hydrothermal methods and its optical properties, Superlattice Microsoft 77, 256–266.

[21] Madhu, G., Bose, V.C., Aiswaryaraj, A.S., Maniammal, K., Biju, V., 2013. Defect dependent antioxidant activity of nanostructured nickel oxide synthesized through a novel chemical method, Colloids Surf. A 429, 44–50.

[22] Avenue, K.G.V, Walford, S. 1996. Composition of cane juice. Proceedings of South African Sugar Technologists Association, 70, 265–266.

[23] Chin, C.J.M., Chen, T.Y., Lee, M., Chang, C.F., Liu, Y.T., Kuo, Y.T. 2014. Effective anodic oxidation of naproxen by platinum nanoparticles coated FTO glass. J. Hazard. Mater., 277, 110–119.

[24] Lekkerkerker-Teunissen, K., Chekol, E.T., Maeng, S.K., Ghebremichael, K., Houtman, C.J., Verliefde, A.R.D., Verberk, J.Q.J.C., Amy, G.L., van Dijk, J. C., 2012. Pharmaceutical removal during managed aquifer recharge with pretreatment by advanced oxidation, Water Sci. Technol. Water Supply. 12, 755-767

[25] Xiu-Shengmiao, Jian-junyang, Metcalfe, C., 2005. Carbamazepine and Its Metabolites in Wastewater and in Biosolids in a Municipal Wastewater Treatment Plant. Environ. Sci. Technol. 39, 7469-7475

[26] Hu, A., Zhang, X., Luong, D., Oakes, K. D., Servos, M. R., Liang, R., Zhou, Y., 2012. Adsorption and photocatalytic degradation kinetics of pharmaceuticals by TiO2 nanowires during water treatment. Waste Biomass Valorization, 3, 443–449.

[27] Li, X., He, Q., Li, H., Gao, X., Hu, M., Li, S., Wang, X., 2017. Bioconversion of non-steroidal anti-inflammatory drugs diclofenac and naproxen by chloroperoxidase. Biochem. Eng. J., 120, 7–16.

[28] Zheng, B., Zheng, Z., Zhang, J., Liu, Q., Wang, J., Luo, X., Wang, L., 2012. Degradation Kinetics and By-Products of Naproxen in Aqueous Solutions by Gamma Irradiation. Environmental Engineering Science, 29(6), 386–391.

[29] Kümmerer, K., 2009. The presence of pharmaceuticals in the environment due to human use - present knowledge and future challenges. J. Environ. Manage, 90(8), 2354–2366.

[30] Santos, L.H.M.L.M., Araújo, A.N., Fachini, A., Pena, A., Delerue-Matos, C., Montenegro, M.C.B.S.M., 2010. Ecotoxicological aspects related to the presence of pharmaceuticals in the aquatic environment. J. Hazard. Mater., 175(1–3), 45–95.

[31] Sarici-Özdemir, C., Önal, Y., 2010. Study to investigate the importance of mass transfer of naproxen sodium onto activated carbon. Chem. Eng. Process. Process Intensif., 49(10), 1058–1065.

[32] Domínguez-Vargas, J.R., Gonzalez, T., Palo, P., Cuerda-Correa, E.M., 2013. Removal of Carbamazepine, Naproxen, and Trimethoprim from Water by Amberlite XAD-7: A Kinetic Study, Clean – Soil, Air, Water. 41, 1052–1061.

[33] Young, R.B., Chefetz, B., Liu, A., Desyaterik, Y., Borch, T., 2014. Direct photodegradation of lamotrigine, (an antiepileptic) in simulated sunlight – pH influenced rates and products. Environ. Sci.: Processes Impacts. 16, 848–857

[34] Challis, J.K., Hanson, M.L., Friesen, K.J., Wong, C.S., 2014. A critical assessment of the photodegradation of pharmaceuticals in aquatic environments: defining our current understanding and identifying knowledge gaps. Environ. Sci.: Processes Impacts 16, 672–696.

[35] Georgaki, I., Vasilaki, E., Katsarakis, N., 2014. A Study on the Degradation of Carbamazepine and Ibuprofen by TiO_2 & ZnO Photocatalysis upon UV/Visible-Light Irradiation. Am J Analyt Chem. 5, 518-534.

[36] Achilleos, A., Hapeshi, E., Xekoukoulotakis, N. P., Mantzavinos, D., Fatta-Kassinos, D., 2010. UV-A and Solar Photodegradationof Ibuprofen and Carbamazepine Catalyzed by TiO_2. Sep. Sci. Technol. 45, 1564–1570.

[37] Karaca, M., Kiranşan, M., Karaca, S., Khataee, A., &Karimi, A., 2016. Sonocatalytic removal of naproxen by synthesized zinc oxide nanoparticles on montmorillonite. Ultrason. Sonochem., 31, 250–256.

[38] Kanakaraju, D., Motti, C. A., Glass, B. D., Oelgemöller, M., 2016. Solar photolysis versus TiO_2-mediated solar photocatalysis: a kinetic study of the degradation of naproxen and diclofenac in various water matrices. Environ. Sci. Pollut. Res., 23(17), 17437–17448.

[40] Bhattacharjee, A., Ahmaruzzaman, M., 2015. Photocatalytic-degradation and reduction of organic compounds using SnO_2 quantum dots (via green route) under direct sunlight. RSC Adv., 5, 66122–66133.

[39] Aoul-hrouz, S., Essamellali, Y., Zahouily, M., 2017. Extraction and Characterization of Lignin from Moroccan Sugarcane Bagasse Using Response Surface Design, Int. J. Trend Res, Dev., 4, 185-191.

[41] Sinha, T., Ahmaruzzaman, M., Adhikari, P.P., Bora, R., 2017. Green and environmentally sustainable fabrication of Ag-SnO_2 nanocomposite and its multifunctional efficacy as photocatalyst and antibacterial and antioxidant agent. ACS Sustainable Chem. Eng., 5, 4645−4655.

[42] Kulkarni, A. A., Bhanage, B. M. 2014. Ag@AgCl nanomaterial synthesis using sugarcane juice and its application in azo dyes degradation. ACS Sustainable Chem. Eng., 2, 1007−1013.

[43] Houas, A., Lachheb, H., Ksibi, M., Elaloui, E., Guillard, C. and Herrmann, J., 2001 Photocatalytic Degradation Pathway of Methylene Blue in Water. Applied Catalysis B: Environmental, 31, 145-157.

[44] Chen, Y., Liu, L., Su, J., Liang, J., Wu, B., Zuo, J., Zuo, Y., 2017. Role of humic substances in the photodegradation of naproxen under simulated sunlight. Chemosphere, 187, 261–267.

[45] Sokół, A., Borowska, K., Karpińska, J., 2017. Investigating the Influence of Some Environmental Factors on the Stability of Paracetamol, Naproxen, and Diclofenac in Simulated Natural Conditions. Pol. J. Environ. Stud., 26(1), 293–302.

[46] Xing, B., Shi, C., Zhang, C., Yi, G., Chen, L., Guo, H., Cao, J. 2016. Preparation of TiO_2 /Activated Carbon Composites for Photocatalytic Degradation of RhB under UV Light Irradiation. Journal of Nanomaterials, 2016, 1–10.

[47] Coria, G., Sirés, I., Brillas, E., Nava, J. L., 2016. Influence of the anode material on the degradation of naproxen by Fenton-based electrochemical processes. Chem. Eng. J., 304, 817–825.

[48] Chen, X., Wu, Z. 2017. Effect of Different Activated Carbon as Carrier on the Photocatalytic Activity of Ag-N-ZnO Photocatalyst for Methyl Orange Degradation under Visible Light Irradiation. Nanomaterials (Basel), 7, 258.

[49] Wang, X.J.; Song, J.K.; Huang, J.Y.; Zhang, J.; Wang, X.; Ma, R.R.; Wang, J.Y.; Zhao, J.F., 2016. Activated carbon-based magnetic TiO_2 photocatalyst co-doped with iodine and nitrogen for organic pollution degradation. Appl. Surf. Sci. 390, 190–201.

List of Figures:

1. Figure 1. (a) UV-visible spectrum of SnO_2/AC nanocomposite (b) plot of $(\alpha h\upsilon)^2$ vs $(h\upsilon)$ for SnO_2/AC nanocomposite.
2. Figure 2. XRD patterns of SnO_2/AC nanocomposite and activated carbon (AC).
3. Figure 3. (a) TEM image, (b) HRTEM images. (c) SAED pattern and (d) particle size distribution histogram of Figure 6. XRD patterns of of SnO_2/AC nanocomposite.
4. Figure 4. FTIR spectra of *Saccharum officinarum* juice, activated carbon (AC) and the synthesized SnO_2/AC nanocomposite
5. Figure 5. EDX spectrum of synthesized of SnO_2/AC nanocomposite.
6. Figure 6. Effect of (a) catalytic loading, (b) initial NPX concentration, (c) Effect of pH of the NPX solution on the photodegradtion process and (d) contact time with SnO_2/AC nanocomposite.
7. Figure 7a. Comparative study of degration of NPX in blank, in dark without and without SnO_2/AC nanocomposite (b) Absorbtion spectra of photodegradation of NPX in dark and under sunlight, (c) percentage efficiency of photodegradation of NPX with time, (d) plot of $\ln(C_0/C)$ versus irradiation time for photodegradation of NPX.
8. Figure 8. Schematic representation of the formation of hole (h^+) and electron (e^-) on the valance band (VB) and conduction band (CB) of SnO_2/AC nanocomposite adsorption and photodegradation of NPX.
9. Figure 9. Recyclability study of synthesized SnO_2/AC nanocomposite degradation of NPX.
10. Figure 10. (a) XRD pattern and (b) TEM micrography of recycled SnO_2/AC nanocomposite after the degradation of NPX.

Figure 1. (a) UV-visible spectrum of SnO_2/AC nanocomposite (b) plot of $(\alpha h\upsilon)^2$ vs $(h\upsilon)$ for SnO_2/AC nanocomposite.

Figure 2. XRD patterns of SnO_2/AC nanocomposite and activated carbon (AC).

.

Figure 3. (a) TEM image, (b) HRTEM images. (c) SAED pattern and (d) particle size distribution histogram of Figure 6. XRD patterns of of SnO_2/AC nanocomposite.

Figure 4. FTIR spectra of *Saccharum officinarum* juice, activated carbon (AC) and synthesized SnO_2/AC nanocomposite

Figure 5. EDX spectrum of synthesized of SnO_2/AC nanocomposite

Figure 6. Effect of (a) catalytic loading, (b) initial NPX concentration, (c) Effect of pH of the NPX solution on the photodegradation process and (d) contact time with SnO_2/AC nanocomposite.

Figure 7a. Comparative study of degration of NPX in blank, in dark without and without SnO_2/AC nanocomposite (b) Absorbtion spectra of photodegradation of NPX in dark and under sunlight, (c) percentage efficiency of photodegradation of NPX with time, (d) plot of $\ln(C_0/C)$ versus irradiation time for photodegradation of NPX.

Figure 8. Schematic representation of the formation of hole (h^+) and electron (e^-) on the valance band (VB) and conduction band (CB) of SnO_2/AC nanocomposite adsorption and photodegradation of NPX.

Figure 9. Recyclability study of synthesized SnO_2/AC nanocomposite degradation of NPX.

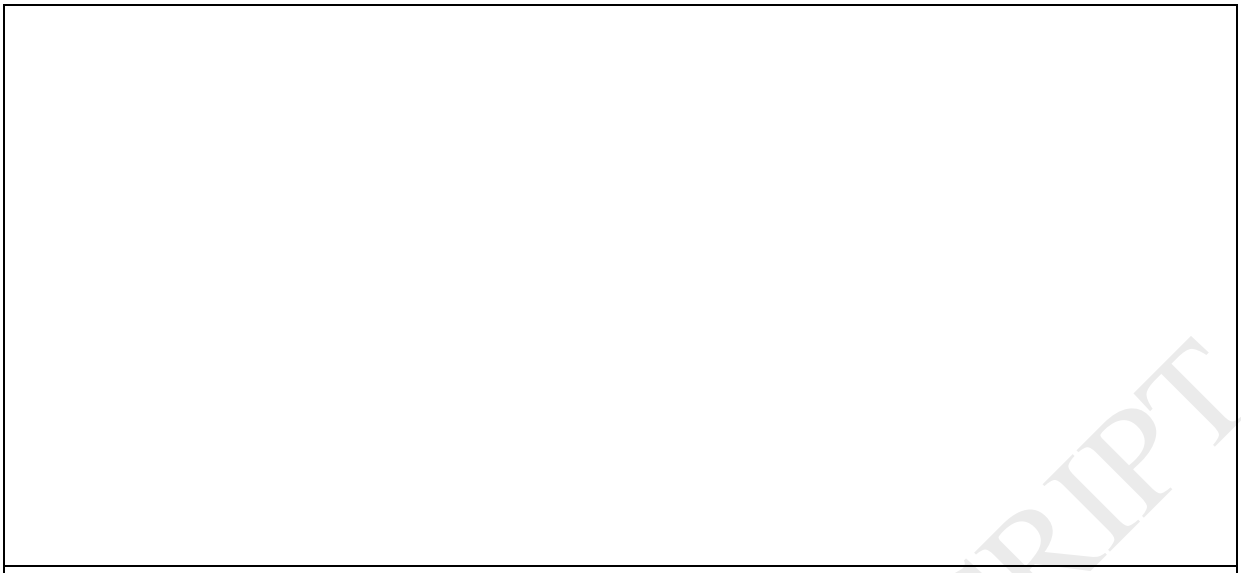

Figure 10. (a) XRD pattern and (b) TEM micrography of recycled SnO_2/AC nanocomposite after the degradation of NPX.

Table 1: Elemental compositions of the SnO_2/AC nanocomposite from EDX spectrum

Element	Weight %	Atomic %
C K	17.32	16.25
O K	41.17	47.93
Mg K	0.83	0.72
Si K	1.09	1.06
P K	0.19	1.06
Cu K	0.60	0.26
Sn L	38.80	33.63
Total	100	